Dynamical charge and structural strain in inorganic fullerenelike MoS_2 nanoparticles

Q.-C. Sun,[1] X. S. Xu,[1] L. I. Vergara,[1] R. Rosentsveig,[2] and J. L. Musfeldt[1]
[1]*Department of Chemistry, University of Tennessee, Knoxville, Tennessee 37996, USA*
[2]*Department of Materials and Interfaces, Weizmann Institute of Science, RehoVot 76100, Israel*
(Received 10 February 2009; published 7 May 2009)

We measured the far-infrared vibrational properties of bulk and nanoscale MoS_2 in order to investigate finite length scale effects and chemical bonding in these materials. From an analysis of frequencies, oscillator strengths, and high-frequency dielectric constants, we extract Born and local effective charges for both materials. In the intralayer direction, we find that the Born effective charge of the nanoparticles is decreased significantly compared to the layered bulk, a difference that we attribute to the structural strain (and resulting change in polarizability) in the nanoparticles.

DOI: 10.1103/PhysRevB.79.205405 PACS number(s): 63.22.Np, 63.20.D−, 78.30.Hv

I. INTRODUCTION

Dimensionality, local structure, and lattice dynamics govern the properties of many complex materials including superconductors, thermoelectrics, and multiferroics.[1–6] Less is known, however, about strain and finite length scale effects in complex materials. There is a special interest in size-shape control of properties and reactivities that depend on an intimate coupling with the lattice.[7–13] New properties and surprising multifunctionalities may also emerge at small length scales.[14–16] Many are a consequence of phonon confinement. In addition to expanding the usable structure-property phase space for tuning functional materials, phonon confinement studies offer the opportunity to probe fundamentally new aspects of structure and chemical bonding in nanomaterials.[17] In this work, we focus on MoS_2, a well-known transition-metal dichalcogenide that was a prototype for foundational studies of charge and bonding in the late 1970s (Refs. 18–20) and continues to support modern tribological applications.[21–23] The discovery and large scale preparation of inorganic fullerenelike (IF) nanostructures[24,25] motivated our detailed analysis of lattice dynamics in IF-MoS_2 nanoparticles.

The structure of 2H-MoS_2 belongs to the $P6_3/mmc$ space group.[26] The atomic centers (six per primitive cell) are arranged in sheets parallel to the base of the hexagonal unit cell [Fig. 1(a)]. One consequence of this architecture is the low-dimensional electronic structure which consists of strong bonding in the *ab* plane and weak van der Waals interactions between layers.[27] Each MoS_2 slab contains a layer of metal centers sandwiched between two chalcogen layers, with each metal atom bonded to six chalcogen atoms in a trigonal prismatic arrangement (D_{3h} local symmetry). Group theory predicts the following irreducible representations: $2A_{2u}+2E_{1u}+A_{1g}+E_{1g}+2E_{2g}+2B_{1g}+B_{2u}+E_{2u}$.[17,27] Displacement vectors of the two infrared-active E_{1u} and A_{2u} modes are shown in Fig. 1(b). These modes are sensitive to charge and bonding in the intralayer and interlayer directions, respectively, and they have been used to assess Born effective charges (Z_B^*) in a number of transition-metal dichalcogenides.[19] For 2H-MoS_2 single crystals, $Z_B^* \approx (1.1-1.2)e$ in the intralayer direction, making it one of the more covalent systems.[18,19] The structure of IF-MoS_2 nanoparticles is similar to that of the nested fullerenes (inset, Fig. 2). X-ray diffraction demonstrates that the bulk 2H- structure is locally preserved within the nanoparticle, albeit with a ~2% *c*-axis expansion.[28,29] We therefore anticipate that the vibrational properties of IF- and 2H-MoS_2 will display similarities befitting their common chemistry, symmetry, and structure and, at the same time, display important differences that derive from confinement, broken translational symmetry, strain, and subtle curvature.[17,30] The connection between charge, structure, and mechanical and tribological properties is still an open question in the IF materials. Recent theoretical work indicates that the substantially reduced friction coefficient under high load conditions has its origins in the local coating processes that take place during particle (or tube) breakup.[13] These breakup processes seem to begin in the inner most highly strained layer of the nanomaterial.

In order to investigate finite length scale effects in model nanomaterials such as the transition-metal dichalcogenides, we measured the far-infrared vibrational properties of IF-MoS_2 nanoparticles and compared the results with the spectrum of the layered bulk counterpart 2H-MoS_2. Vibrational spectroscopy provides a sensitive and microscopic probe of the unique charge and bonding interactions present in the nanomaterial interactions that we quantify by calculating both Born and local effective charges. Application of these traditional models to nanomaterials requires density

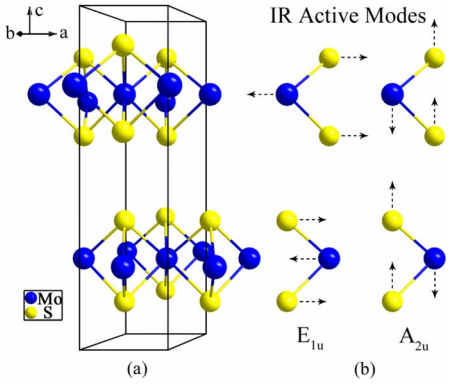

FIG. 1. (Color online) Crystal structure (Ref. 26) and displacement patterns of infrared-active E_{1u} and A_{2u} vibrational modes (Ref. 27) in 2H-MoS_2.

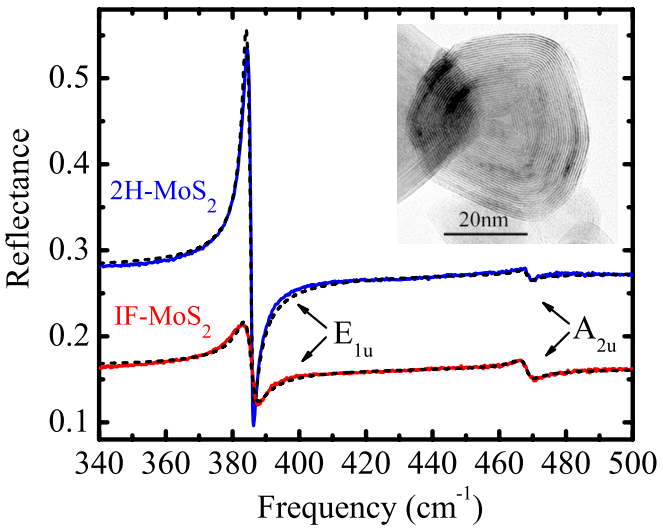

FIG. 2. (Color online) Close-up view of the 300 K reflectance spectra of bulk and nanoscale MoS_2. Blue (upper) and red (lower) curves: experimental data for the 2H- and IF-MoS_2 samples, respectively. Black dashed lines: theoretical fits as described in the text. Inset: high-resolution transmission electron microscopy image of IF-MoS_2 showing the lattice fringing and curvature in the nanoparticles. The layer-to-layer distance is 0.62 nm.

and orientational corrections, modifications to the method that we detail here. We find that the intralayer Born effective charge decreases strongly in IF-MoS_2 compared to the 2H counterpart. Comparison with local effective charge values demonstrates that this decrease is due to the structural strain and the consequent modification of intralayer polarizability that reduces nonlocal effective charge in the nanomaterial.

II. EXPERIMENTAL METHODS

IF-MoS_2 was synthesized by a gas phase reaction from MoO_3 powder by a three-step procedure in a vertical bed reactor.[31] The resulting nanoparticles ranged in size from ~30–70 nm in diameter (inset, Fig. 2). 2H-MoS_2 was purchased directly from Alfa Aesar (99%). Pressed isotropic pellets of the 2H- and IF-MoS_2 powder were prepared for investigating their dynamical properties. Note that the theoretical calculated density of 2H-MoS_2 single crystal is 4.996 g/cm^3, and the actual densities of bulk and IF pellets are ~3.5 g/cm^3. Pellet densities are therefore ~70% of the single-crystal density, a difference that we correct for in our analysis.[32] Near normal infrared reflectance was measured over a wide frequency range using a series of spectrometers including a Bruker 113V Fourier transform infrared spectrometer, an Equinox 55 Fourier transform instrument (equipped with a microscope attachment), and a Perkin Elmer Lambda 900 grating spectrometer, covering the frequency range from 25–52 000 cm^{-1}. A helium-cooled bolometer detector was employed in the far infrared for added sensitivity. 0.5 cm^{-1} resolution was used in the infrared, whereas 3 nm resolution was employed in the optical regime. A Lorentzian oscillator analysis was used to (i) fit the measured reflectance and (ii) calculate the optical constants from the extracted parameters, yielding information on the dispersive and lossy response of each material.[33] A Kramers-Kronig analysis can also be used to obtain the optical constants.[34]

III. RESULTS AND DISCUSSION

Figure 2 shows a close-up view of the far-infrared reflectance spectra of 2H- and IF-MoS_2 at 300 K. Two vibrational modes are observed, in agreement with group theory predictions.[17,27] We assign the peak at 384 cm^{-1} to the E_{1u} optical mode and the feature near 468 cm^{-1} to the A_{2u} optical mode. These spectral features probe intralayer and interlayer dynamics, respectively. The observed band positions are in reasonable agreement with previous single-crystal data[18] and similar pressed pellet results on bulk and nanoscale WS_2 (with appropriate mass correction).[17] The character of the E_{1u} and A_{2u} modes is strikingly different in the two materials. In IF-MoS_2, the E_{1u} mode is damped and suppressed compared to the 2H- analog, whereas the A_{2u} mode is slightly more pronounced in the IF- compound compared to that in the bulk. These differences can be quantified using classical dielectric oscillator models and fitting techniques.[20,35]

We employed classical Lorentz models to fit the reflectance spectra of 2H- and IF-MoS_2 with a complex dielectric constant $\varepsilon(\omega)=\varepsilon_1(\omega)+i\varepsilon_2(\omega)$ constructed as a superposition of Lorentzian oscillators as[20,35]

$$\varepsilon(\omega) = \sum_j \frac{S_j \omega_{\mathrm{TO},j}^2}{(\omega_{\mathrm{TO},j}^2 - \omega^2) - i\gamma_j\omega} + \varepsilon(\infty). \quad (1)$$

Here, S is the oscillator strength, ω_{TO} is the transverse optical phonon frequency, γ is the damping constant, $\varepsilon(\infty)$ is the high-frequency dielectric constant, and j is the mode index. Good quality fits were obtained using a total of two oscillators, as shown in Fig. 2. These data are summarized in Table I as a set of "observed parameters," where the observed oscillator strength and dielectric constant are actually tabulated as $\bar{S}$ and $\bar{\varepsilon}(\infty)$ to distinguish these powder averages from the density- and distribution-corrected values discussed later. From these fits, we calculated the optical constants of 2H- and IF-MoS_2. Optical constants can also be calculated with a Kramers-Kronig analysis.

The rigid-ion model[36,37] gives a precise relationship between the longitudinal and transverse optic phonon frequencies (often called the LO-TO splitting)[38] and Born effective charge,

$$4\pi^2 c^2 \sum_j (\omega_{\mathrm{LO},j}^2 - \omega_{\mathrm{TO},j}^2) = \frac{Ne^2}{\epsilon_0 \varepsilon(\infty) V} \sum_k \frac{(Z_{B,k}^*)^2}{m_k}. \quad (2)$$

Here, $\omega_{\mathrm{LO},j}$ is the longitudinal-optic phonon frequency for the jth oscillator, $Z_{B,k}^*$ is the dimensionless Born effective charge on the kth ion, N is the number of formula units in the unit cell, V is the volume of the MoS_2 formula unit, m_k is the atomic mass of the kth atom, ϵ_0 is the permittivity of free space, e is the electronic charge, and c is the speed of light. The sum rule $\Sigma Z_{B,k}^*=0$ guarantees that the charge neutrality

TABLE I. Observed and scaled parameters extracted from our oscillator fitting analysis of the measured reflectance spectra of 2H- and IF-MoS_2.

Material	Mode	$\bar{S}_j$ [a] $\times 10^{-3}$	$\bar{\varepsilon}(\infty)$ [a]	S_j $\times 10^{-3}$	$\varepsilon(\infty)$	$\omega_{\mathrm{TO},j}$ (cm^{-1})
2H-MoS_2 (Crystal)	E_{1u}			200[b]	15.2[b]	384[b]
	A_{2u}			30[b]	6.2[b]	470[b]
2H-MoS_2 (Powder)	E_{1u}	114	10.3	200[c]	15.2[c]	383.7[a]
	A_{2u}	3.6		30[c]	6.2[c]	468.2[a]
IF-MoS_2 (Powder)	E_{1u}	36	5.6	77[c]	8.3[c]	384.6[a]
	A_{2u}	6.7		29[c]	6.2[c]	467.9[a]

[a]Observed parameters extracted from our oscillator fitting analysis of the measured reflectance spectra (Fig. 2).
[b]Single-crystal data from Ref. 18.
[c]Effective oscillator strength and dielectric constant obtained by correcting the observed powder data for density and orientational averaging.

condition is fulfilled. In other words, the sum of Born effective charges for all atoms in the unit cell must vanish, element by element.[39] Unfortunately, Eq. (2) is valid only when the LO-TO splitting of a single-crystal sample is known. Thus, it is not well suited for assessing charge and bonding in nanomaterials as the latter is often in powder form. We can finesse this problem by employing oscillator strength changes rather than LO-TO splitting, as described below. This procedure allows us to calculate pseudo-Born effective charges for both 2H- and IF-MoS_2. These values can be compared with the known Born effective charge in the 2H- single crystal [$Z_B^* \approx (1.1-1.2)e$ in the intralayer direction[18,19]], providing an effective check for our method.

Equation (1) and the generalized Lyddane-Sachs-Teller relationship[40] provide a way forward by articulating the relationship between dielectric constant, oscillator strength, and the LO-TO splitting $\varepsilon(\infty)\cdot(\omega_{\mathrm{LO},j}^2-\omega_{\mathrm{TO},j}^2)=\omega_{\mathrm{TO},j}^2\cdot S_j$.[33] Substituting this result into Eq. (2), we see that Born effective charge can also be calculated mode by mode from the knowledge of oscillator strength,

$$4\pi^2c^2\omega_{\mathrm{TO},j}^2\sum_j S_j = \frac{Ne^2}{\epsilon_0 V}\sum_k \frac{(Z_{B,k}^*)^2}{m_k}. \tag{3}$$

This rendering is well suited to the analysis of nanomaterials and will be employed in this work to evaluate charge and bonding in IF-MoS_2 nanoparticles.

Before presenting the results of this analysis for the nanoparticles, we briefly point out that the dynamical charge values extracted from our analysis of the 2H-MoS_2 pressed pellet sample are in good agreement with single-crystal results from the literature.[18,19] This agreement provides confidence that the formulation presented in Eq. (3) can be extended in a powerful way to include nanomaterials. That the sample is in powder form presents two main challenges: (i) the pressed pellet density is less than that of the corresponding single crystal thus underestimating the intrinsic oscillator strength of each infrared-active vibrational mode and (ii) the spatial distribution of the dipole moment operator in a powder sample is not that of a single crystal, an effect that also works to misrepresent oscillator strength. The density correction merely scales the observed oscillator strength toward its intrinsic value. The spatial distribution correction is more complex. This is because in some samples, there may be a random orientation (such as the nanoparticles in this work). In other samples, for instance 2H-MoS_2, the orientation correction must account for the powdered nature of an anisotropic sample and the preferential surface orientation of the platelets in a pressed pellet sample. Here is how it works. When an oscillator has an angle θ with respect to the macroscopic field E, the observed oscillator strength ($\bar{S}$) will be reduced compared to its intrinsic value (S). Employing both Eq. (1) and the definition of electric displacement [$D=\epsilon_0 E+P=\varepsilon(\omega)\epsilon_0 E$], three useful expressions can be obtained which capture and compensate for the inherent orientational aspects in MoS_2 or any similar two-dimensional material in powder form,[33]

$$\bar{S}_{E_{1u}} = S_{E_{1u}}\langle\cos^2(\theta_{E_{1u}})\rangle v, \tag{4a}$$

$$\bar{S}_{A_{2u}} = S_{A_{2u}}\langle\cos^2(\theta_{A_{2u}})\rangle v, \tag{4b}$$

$$\bar{\varepsilon}(\infty) = 1 + [\varepsilon_{E_{1u}}(\infty)-1]\langle\cos^2(\theta_{E_{1u}})\rangle v + [\varepsilon_{A_{2u}}(\infty)-1] \times\langle\cos^2(\theta_{A_{2u}})\rangle v. \tag{4c}$$

Here, v is the relative density of a powdered vs single-crystalline sample. In this work, $v=0.70$.[32] From Eqs. (4a) and (4b), it may appear that both $\langle\cos^2(\theta_{E_{1u}})\rangle$ and $\langle\cos^2(\theta_{A_{2u}})\rangle$ are unknown. However, in the 2H material, the two modes in question are orthogonal. Thus, $\theta_{E_{1u}}+\theta_{A_{2u}}=\frac{\pi}{2}$ and $\langle\cos^2(\theta_{E_{1u}})\rangle+\langle\cos^2(\theta_{A_{2u}})\rangle=1$. Thus, there is really only one unknown. We can find the value of $\langle\cos^2(\theta_{E_{1u}})\rangle$ by comparison with Wieting and Verble's[18] 2H-MoS_2 single-crystal data. As shown in Table I, $S_{E_{1u}}=0.20$, $S_{A_{2u}}=0.03$, $\varepsilon_{E_{1u}}(\infty)=15.2$, and $\varepsilon_{A_{2u}}(\infty)=6.2$. These parameters ought to be applicable to a powder sample as long as surface effects are not too important. As discussed previously, fits to our powder data yielded $\bar{S}_{E_{1u}}=0.114$, $\bar{S}_{A_{2u}}=0.0036$, and $\bar{\varepsilon}(\infty)=10.3$ (Table I). Working backward with Eqs. (4a) and (4b), we extract independent estimates of $\langle\cos^2(\theta_{E_{1u}})\rangle$ from the analysis of the E_{1u} and A_{2u} modes as 0.81 and 0.83, respectively.[41,42] Using Eq. (4c) and an average value of $\langle\cos^2(\theta_{E_{1u}})\rangle=0.82$, we extract $\bar{\varepsilon}(\infty)=9.8$, consistent with that obtained by direct fitting techniques [$\bar{\varepsilon}(\infty)=10.3$]. Finally, we employ Eq. (3) and the aforementioned effective parameters to calculate the Born effective charges. We find $Z_B^*=1.11e$ and $0.52e$, in the intralayer and interlayer directions, respectively. Here, we explicitly show the charge of the electron because it is traditional to do so. This analysis

TABLE II. Effective charges and other parameters of 2H- and IF-MoS_2 in the two principle directions.

Mode	Material	Z_B^* (e)	$\varepsilon(\infty)$	n	α (Å^3)	Z^* (e)
E_{1u}	2H	1.11	15.2	0.461	100	0.15
	IF	0.69	8.3	0.462	91	0.16
A_{2u}	2H	0.52	6.2	0.078	200	0.37
	IF	0.52	6.2	0.076	200	0.37

shows that the optical constants of 2H powder and single-crystalline[18,19] samples are identical, as they should be, once density and orientational effects are taken into account. It also demonstrates that the approach outlined here can be reliably extended to analyze nanomaterials.

We can carry out the same analysis for the nanoparticles. Table I displays the results of our fit to the powder spectra for IF-MoS_2. Using this data [$\bar{S}_{E_{1u}}=0.036$, $\bar{S}_{A_{2u}}=0.0067$, and $\bar{\varepsilon}(\infty)=5.6$], we evaluate the important quantities as discussed above. Assuming spherical nanoparticles,[43] we obtain $\langle\cos^2(\theta_{E_{1u}})\rangle=\int(\sin^3\theta)d\theta=\frac{2}{3}$ and $\langle\cos^2(\theta_{A_{2u}})\rangle=\int(\cos^2\theta)\sin\theta d\theta=\frac{1}{3}$. Inserting these values into Eqs. (4a) and (4b), we find $S_{E_{1u}}=0.077$ and $S_{A_{2u}}=0.029$. As before, a density factor of 0.70 has been applied to account for the reduced density of the pressed pellet sample. Using Eq. (3) and these effective parameters, we calculate the Born effective charges for the infrared-active phonon modes of IF-MoS_2. We find $Z_B^*=0.69e$ in the intralayer direction, significantly less than that obtained for the 2H material. In the interlayer direction, we extract $Z_B^*=0.52e$, identical to that obtained for the layered bulk.

These results are summarized in Table II. In the intralayer direction, the Born effective charge of the Mo center decreases from $1.11e$ in the bulk material to $0.69e$ in the nanoparticles. In the interlayer direction, Z_B^* is unchanged ($\sim 0.52e$) within our sensitivity. The origin of these trends is discussed below.

The vibrational response of 2H- and IF-MoS_2 (Fig. 2) can be also used to extract information about the structural strain in the nanoparticles and elucidate the consequences for bonding, polarizability, local, and nonlocal effective charges. In an ionic solid, we need to consider the so-called depolarization field, which originates from the influence of neighboring ions. The polarization $P=\frac{N}{V}(Z^*x+\alpha E_{\text{eff}})$ has two parts. The first contribution is due to the relative displacements of ions. The second results from the electron cloud distortion around the polarizable ionic centers due to the macroscopic electric field E. Here, Z^* is the local effective charge (or dynamic ionic charge), α is the polarizability in one direction of the unit cell, E_{eff} is the microscopic electric field ($E_{\text{eff}}=E+\frac{n}{\epsilon_0}P$), n is the depolarization factor, and P is the polarization.[44–46] Using these relationships, we can evaluate local effective charges and polarizabilites for both materials as[33]

$$Z_B^*=\frac{Z^*}{1-n\frac{N\alpha}{V}}, \tag{5a}$$

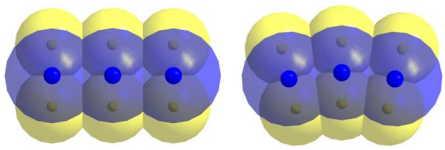

2H IF

FIG. 3. (Color online) Schematic view of the electron clouds of 2H- and IF-MoS_2 in the intralayer direction, respectively. Here, we use spheres to indicate a generalized orbital.

$$\varepsilon(\infty)=1+\frac{\frac{N\alpha}{V}}{1-n\frac{N\alpha}{V}}. \tag{5b}$$

These equations provide a more comprehensive definition of the local effective charge compared to earlier presentations by Uchida and Tanaka[19] and Lucovsky *et al.*[47] Although the previous authors considered the depolarization field (and captured the effect of dipole-dipole interactions), they employed the macroscopic electric field E rather than the microscopic field E_{eff} to evaluate the polarization, resulting in an overestimation of the local effective charge.

Using Eqs. (5a) and (5b), we can calculate the local effective charge and polarizability for 2H-MoS_2.[48] We find $Z^*=0.15e$ and $\alpha=100$ Å^3 in the intralayer direction. For IF-MoS_2, we employ the same equations and the effective dielectric data in Table I to extract the local effective charge and intralayer polarizability as $Z^*=0.16e$ and $\alpha=91$ Å^3, respectively. Here, we explicitly include the electron charge because it is common to do so. These results are summarized in Table II. This analysis demonstrates that the intralayer local effective charge is unaffected by strain and curvature in the nanomaterial. Interpreting the results in terms of chemical bonding, it shows that these chemically identical but morphologically different materials have the same ionicity. In other words, chemical bonding is the same.

In light of this null result, how should we understand the significant decrease in the intralayer Born effective charge of the nanomaterial? The answer lies with the polarizability, a quantity that captures electron cloud distortion effects. Based upon our extracted values of α for 2H- and IF-MoS_2, we can see that the intralayer Born effective charge decreases significantly in the nanomaterial due to a change in intralayer polarizability (Table II). Figure 3 displays a schematic view of the effect of structural strain on the intralayer electron cloud of bulk and nanoscale MoS_2. It is this type of electron cloud distortion that reduces intralayer polarizability in IF-MoS_2. Since the total charge=local charge +nonlocal charge, the electron cloud distortion can be considered to decrease the nonlocal effective charge in the nanoparticles.

The absence of substantial charge and bonding differences in the interlayer direction of the nanomaterial is consistent with the weak van der Waals interactions between layers in transition-metal dichalcogenides. In the interlayer direction, curvature simply has a limited effect on the Born effective charge in IF-MoS_2. Thus, we surmise that the interlayer polarizability remains relatively unchanged in the nanomaterial, and as a consequence, that the local effective charge is the

same for both materials in the interlayer direction (Table II). Dielectric constant data (Table I) are consistent with this conclusion.[49]

We can employ a Hooke's law analysis to extract the force constant k as

$$\omega_{\mathrm{TO}}^2 = \left[\omega_0^2 - \frac{\frac{N}{\epsilon_0}\frac{n(Z^*)^2}{\mu V}}{1 - n\frac{N\alpha}{V}} \right]. \quad (6)$$

Here, ω_0 is the spring-constant frequency ($\omega_0^2 = \frac{k}{\mu}$), and μ is the reduced mass. For both materials, we find $k = 338$ N/m for the E_{1u} mode and $k = 497$ N/m for the A_{2u} mode, again demonstrating that while chemical bonding does not change, strain and curvature in the nanoparticles does affect ionic polarizability.

Finally, we point out that in addition to quantifying bulk vs nanoscale effects and assessing the size dependence of charge and bonding in nanoparticles, these techniques can be extended to include shape effects. MoS_2 nanotubes and nanobuds are the chemically identical "high aspect ratio" analogs in this case.[23,50] At this time, sufficient quantities of material are not available to support an extended investigation.

IV. CONCLUSION

To summarize, we measured the far-infrared vibrational properties of IF-MoS_2 nanoparticles and compared the results with the spectrum of the layered bulk counterpart 2H-MoS_2 in order to investigate finite length scale effects in model transition-metal dichalcogenide nanomaterials. Vibrational spectroscopy provides a sensitive and microscopic probe of the unique charge and bonding interactions present in the nanomaterial, interactions that we quantify by calculating both Born and local effective charges. We find that the intralayer Born effective charge decreases strongly in IF-MoS_2 compared to the 2H counterpart, whereas it remains unchanged in the interlayer direction. Comparison with the local effective charge and polarizability demonstrates that this decrease is due to the structural strain and the consequent modification of the intralayer polarizability that reduces the nonlocal effective charge in the nanoscale material.

ACKNOWLEDGMENTS

This work was supported by the Material Science Division, Basic Energy Sciences, U.S. Department of Energy under Contract No. DE-FG02-01ER45885 (UT), the Joint Directed Research and Development Program (UT), and NanoMaterials, Ltd. (Weizmann). We thank Reshef Tenne for very useful discussions and Yishai Feldman, Ran Vardimon, and Olga Sima for the x-ray work.

[1] C. C. Homes, S. V. Dordevic, G. D. Gu, Q. Li, T. Valla, and J. M. Tranquada, Phys. Rev. Lett. **96**, 257002 (2006).
[2] P. F. P. Poudeu, J. D'Angelo, A. D. Downey, J. L. Short, T. P. Hogan, and M. G. Kanatzidis, Angew. Chem., Int. Ed. **45**, 3835 (2006).
[3] A. I. Hochbaum, R. K. Chen, R. D. Delgado, W. J. Liang, E. C. Garnett, M. Najarian, A. Majumdar, and P. D. Yang, Nature (London) **451**, 163 (2008).
[4] A. I. Boukai, Y. Bunimovich, J. Tahir-Kheli, J. K. Yu, W. A. Goddard, and J. R. Heath, Nature (London) **451**, 168 (2008).
[5] J. Cao, L. I. Vergara, J. L. Musfeldt, A. P. Litvinchuk, Y. J. Wang, S. Park, and S. W. Cheong, Phys. Rev. Lett. **100**, 177205 (2008).
[6] H. Barath, M. Kim, J. F. Karpus, S. L. Cooper, P. Abbamonte, E. Fradkin, E. Morosan, and R. J. Cava, Phys. Rev. Lett. **100**, 106402 (2008).
[7] X. Peng, L. Manna, W. D. Yang, J. Wickham, E. Scher, A. Kadavanich, and A. P. Alivisatos, Nature (London) **404**, 59 (2000).
[8] V. F. Puntes, K. M. Krishnan, and A. P. Alivisatos, Science **291**, 2115 (2001).
[9] S. Brown, J. L. Musfeldt, I. Mihut, J. B. Betts, A. Migliori, A. Zak, and R. Tenne, Nano Lett. **7**, 2365 (2007).
[10] C. C. Li, K. L. Shuford, Q. H. Park, W. P. Cai, Y. Li, E. J. Lee, and S. O. Cho, Angew. Chem., Int. Ed. **46**, 3264 (2007).
[11] M. Okubo, E. Hosono, J. Kim, M. Enomoto, N. Kojima, T. Kudo, H. S. Zhou, and I. Honma, J. Am. Chem. Soc. **129**, 7444 (2007).
[12] I. Rusakova, T. Ould-Ely, C. Hofmann, D. Prieto-Centurion, C. S. Levin, N. J. Halas, A. Luttge, and K. H. Whitmire, Chem. Mater. **19**, 1369 (2007).
[13] M. Stefanov, A. N. Enyashin, T. Heine, and G. Seifert, J. Phys. Chem. C **112**, 17764 (2008).
[14] J. W. Long and D. R. Rolison, Acc. Chem. Res. **40**, 854 (2007).
[15] B. Poudel, Q. Hao, Y. Ma, Y. C. Lan, A. Minnich, B. Yu, X. Yan, D. Z. Wang, A. Muto, D. Vashaee, X. Y. Chen, J. M. Liu, M. S. Dresselhaus, G. Chen, and Z. F. Ren, Science **320**, 634 (2008).
[16] S. Y. Quek, M. M. Biener, J. Biener, J. Bhattacharjee, C. M. Friend, U. V. Waghmare, and E. Kaxiras, J. Chem. Phys. **127**, 104704 (2007).
[17] R. D. Luttrell, S. Brown, J. Cao, J. L. Musfeldt, R. Rosentsveig, and R. Tenne, Phys. Rev. B **73**, 035410 (2006).
[18] T. J. Wieting and J. L. Verble, Phys. Rev. B **3**, 4286 (1971).
[19] S. I. Uchida and S. Tanaka, J. Phys. Soc. Jpn. **45**, 153 (1978).
[20] G. Lucovsky, R. M. White, J. A. Benda, and J. F. Revelli, Phys. Rev. B **7**, 3859 (1973).
[21] L. Rapoport, Y. Bilik, Y. Feldman, M. Homyonfer, S. R. Cohen, and R. Tenne, Nature (London) **387**, 791 (1997).
[22] G. Seifert, H. Terrones, M. Terrones, G. Jungnickel, and T. Frauenheim, Phys. Rev. Lett. **85**, 146 (2000).
[23] M. Remškar, A. Mrzel, M. Viršek, and A. Jesih, Adv. Mater. (Weinheim, Ger.) **19**, 4276 (2007).
[24] R. Tenne, L. Margulis, M. Genut, and G. Hodes, Nature (London) **360**, 444 (1992).
[25] L. Margulis, G. Salitra, R. Tenne, and M. Talianker, Nature (London) **365**, 113 (1993).
[26] B. Schonfeld, J. J. Huang, and S. C. Moss, Acta Crystallogr., Sect. B: Struct. Sci. **39**, 404 (1983).
[27] J. L. Verble and T. J. Wieting, Phys. Rev. Lett. **25**, 362 (1970).

[28] Y. Feldman, G. L. Frey, M. Homyonfer, V. Lyakhovitskaya, L. Margulis, H. Cohen, G. Hodes, J. L. Hutchison, and R. Tenne, J. Am. Chem. Soc. **118**, 5362 (1996).
[29] G. L. Frey, S. Elani, M. Homyonfer, Y. Feldman, and R. Tenne, Phys. Rev. B **57**, 6666 (1998).
[30] G. L. Frey, R. Tenne, M. J. Matthews, M. S. Dresselhaus, and G. Dresselhaus, Phys. Rev. B **60**, 2883 (1999).
[31] A. Zak, Y. Feldman, V. Alperovich, R. Rosentsveig, and R. Tenne, J. Am. Chem. Soc. **122**, 11108 (2000).
[32] Pellets were prepared with very modest pressure, so we do not anticipate that the density will approach that of a single crystal as it would if high pressures were employed.
[33] X. S. Xu, Q.-C. Sun, and J. L. Musfeldt, arXiv:0904.3322v1 (unpublished).
[34] F. Wooten, *Optical Properties of Solids* (Academic Press, New York, 1972).
[35] R. Zallen, M. L. Slade, and A. T. Ward, Phys. Rev. B **3**, 4257 (1971).
[36] R. Resta, M. Posternak, and A. Baldereschi, Phys. Rev. Lett. **70**, 1010 (1993).
[37] K. W. Lee and W. E. Pickett, Phys. Rev. B **68**, 085308 (2003).
[38] LO-TO splitting is a specific feature of a polar material and represents a measure of coupling with the electric field screened by the electrons.
[39] X. Gonze and C. Lee, Phys. Rev. B **55**, 10355 (1997).
[40] N. W. Ashcroft and N. D. Mermin, *Solid State Physics* (Thomson Learning, New York, 1976).
[41] This indicates a slight surface orientation of the platelets in the pressed pellet samples, as anticipated.
[42] An independent x-ray measurement verified this estimate of orientation.
[43] This assumption is not strictly true. TEM images show that the nanoparticles can have a few "corners," although for practical purposes, neglect of corners and the hierarchy of length scales in these MoS_2 nanoparticles is a reasonable assumption.
[44] K. Huang and R. Q. Han, *Solid State Physics* (Higher Education, China, 1988).
[45] M. Born and K. Huang, *Dynamical Theory of Crystal Lattices* (Oxford University Press, London, 1954).
[46] L. D. Landau, E. M. Lifshitz, and L. P. Pitaevskii, *Electrodynamics of Continuous Media*, 2nd ed. (Butterworth-Heinemann, New York, 1984).
[47] G. Lucovsky, R. M. Martin, and E. Burstein, Phys. Rev. B **4**, 1367 (1971).
[48] The depolarization factor for anisotropic materials was given by Landau (Ref. 46).
[49] Based on our assumption that the interlayer polarizability of IF is the same as 2H, $\varepsilon_{A_{2u}}(\infty)=6.2$ for IF. Then using Eq. (4c) and fitting result $\bar{\varepsilon}(\infty)=5.6$ of IF, we got $\varepsilon_{E_{1u}}(\infty)=8.3$, which were shown in Table I.
[50] Y. Feldman, E. Wasserman, D. J. Srolovitz, and R. Tenne, Science **267**, 222 (1995).